Metrol. Meas. Syst., Vol. XVII (2010), No. 3, pp. 363-382

PAN POLSKA AKADEMIA NAUK

METROLOGY AND MEASUREMENT SYSTEMS

Index 330930, ISSN 0860-8229

www.metrology.pg.gda.pl

M&MS

DISTRIBUTION MEASUREMENTS OF RADII OF DROPLETS FORMING AN EXPLOSIVELY GENERATED WATER-SPRAY CLOUD

Dariusz Chaberski[1)], Sławomir Grzelak[1)], Damian Lewandowski[2)], Roman Dygdała[2,5)], Marek Zieliński[1,3)], Krzysztof Stefański[4)], Grzegorz Śmigielski[3)]

1) Nicolaus Copernicus University, Institute of Physics, Grudziądzka 5, 87-100 Toruń, Poland (daras@fizyka.umk.pl, ✉ slawg@fizyka.umk.pl, +48 56 611 3324, marziel@fizyka.umk.pl)
2) Paweł Włodkowic University College in Plock, Al. Kilińskiego 12, 09-402 Płock, Poland (damian_lew2@wp.pl)
3) The University of Economy, Garbary 2, 85-067 Bydgoszcz, Poland (gsmigielski@byd.pl)
4) Collegium Medicum, Nicolaus Copernicus University, Jagiellońska 13-15, 85-067 Bydgoszcz (stefan@fizyka.umk.pl)
5) Kazimierz Wielki University, Institute of Physics Plac Weyssenhoffa 11, 85-072 Bydgoszcz (romdy1@onet.pl)

Abstract

Three methods of estimating radii of spray droplets are discussed and results of their practical application in the case of explosively produced water spray are reported. Parameters of model radii distributions are fitted using the least squares method. Finally, the data obtained for a number of tests are used for estimating fraction of explosion energy used for pulverization of water in the process of explosive production of water-spray.

Keywords: spray droplets, radii distribution, pulverization energy, fire extinguishing.

1. Introduction

Fire extinguishing properties of water spray are well known and from some time they are used in extinguishing small and medium-size fires [1, 2]. The size of the spray droplets is one of the crucial factors influencing the effectiveness of fire-quenching. Therefore measurement of droplet sizes is one of the introductory tests of the quality of a spray-producing device. Technical solutions used for producing water-spray for such purpose cannot, however, be simply scaled-up to make devices suitable for extinguishing large-scale fires.

Although a fire-extinguishing machine designed for quenching large scale fires must comprise many components like the high precision air-delivery system [3], explosive production of water-spray is its core [4, 5]. Determination of the explosion energy distribution among the basic dissipation channels is one of the crucial problems for modelling the process of production of the spray.

As was shown in our previous papers [6, 7], knowledge of the distribution of diameters of droplets allows one to estimate the part of the energy used for pulverization of water. It is rather difficult to compute such a distribution theoretically since even if one can model its shape, parameter values must be determined by experiments [8]. Therefore, development of experimental techniques allowing one to determine it, is of crucial importance.

Some research of this sort had been done before. Stebnovskii [8] has reported results of distribution of droplets' size measurements obtained with quite clever and elaborate equipment including a trapping device in which droplets are collected on an immersion covered plate. His experiments, however, had been performed for about 5 g of explosive material and less than 100 g of water. Such a small scale allowed to run the experiment inside a bucket-size cylindrical chamber located inside the laboratory. The results allowed to shed

Article history: received on Jun. 7, 2010; accepted on Sept. 05, 2010; available online on Sept. 6, 2010.

light on the initial stage of expansion of the foam-like liquid and on the process of its fragmentation.

The tests whose results are reported in this paper had been run with amounts of explosive material and water exceeding those used by Stebnovskii by about three orders of magnitude. The scale entailed, on the one hand, some limitations and, on the other hand, opened some new possibilities. The tests had to be run in the open air, and measurements had to be made at least 5 m from the axis of explosion. On the other hand essential parameters could be measured at distances at least an order of magnitude larger than in the case of Stebnovskii's micro-scale spray generator.

In this paper in Section 2 we give formulae describing the relation between the energy used for pulverization of water and the distribution of the radii of the resulting water droplets. Section 3 is devoted to a general review of phenomena allowing one to estimate droplets' diameters. In Section 4 we discuss results of measurements of droplets using various methods. In Section 5 we present the reconstruction of a model radii distribution from experimental data. Results of pulverization energy estimation are shown in Section 6. Finally, in Section 7 we present a discussion of the results and conclusions.

2. Droplets' radii distribution and pulverization energy

As was shown in other papers [6, 7], the total energy of explosion is dissipated into three channels: the pulverization channel, the acceleration channel and the loss channel. This classification is strictly connected with the objective of explosive dispersion of water: production of droplets as small as possible and giving them the axifugal velocity as large as possible. The part of explosion energy not used for either of these purposes, *i.e.* the lost energy E_{loss} is stored in the shock-wave overrunning the expanding water-spray cloud.

The pulverization energy can be computed using the total outer area of all droplets and the surface tension coefficient. The acceleration energy can be estimated using the distribution of droplets' velocities and the total mass of the water. Finally the lost energy may be estimated using parameters of the shock-wave.

Here we will focus our attention on the estimation of the pulverization energy, which is, in a way, the simplest one. One can estimate this energy by the potential energy of the surface tension of all droplets generated in the process of explosion. In the case of fragmentation of the water bulk into N identical droplets one would have:

$$S_N = N^{\frac{1}{3}} S_0, \tag{1}$$

where S_N is the outer area of a single droplet and S_0 is the outer area of the initial water bulk of approximately spherical shape.

In practice, one does not obtain identical droplets in the process of pulverization. Their radii should exhibit a certain distribution instead. One can describe it in the form:

$$\rho(r) = \alpha \rho_p(r), \tag{2}$$

where ρ_p *i*s the probability density function fulfilling the normalization condition:

$$\int_0^\infty \rho_p(r) dr = 1, \tag{3}$$

and coefficient α guarantees fulfillment by the distribution function ρ of the condition:

$$\int_0^\infty \rho(r)V(r)dr = V_0\,, \tag{4}$$

which follows from the assumption that the total volume of water V_0 must be preserved. Assuming a spherical shape of droplets and taking the radius of the ball of the initial volume R, one has:

$$V(r) = 4\pi r^3/3 \text{ and } V_0 = 4\pi R^3/3. \tag{5}$$

After substituting (5) into (4) the formula:

$$\alpha\int_0^\infty \rho_p(r)r^3dr = R^3 \tag{6}$$

is obtained. Taking into account that:

$$\int_0^\infty \rho_p(r)r^3dr = m_3\,, \tag{7}$$

i.e., it is the third order ordinary moment of the probability density function, one gets the flowing formula for the weighting coefficient α:

$$\alpha = R^3/m_3\,. \tag{8}$$

The total area of the spray droplets in such a case is given by the formula:

$$A_{tot} = \int_0^\infty \rho(r)A(r)dr\,, \tag{9}$$

where:

$$A(r) = 4\pi r^2\,. \tag{10}$$

As such:

$$A_{tot} = \alpha\int_0^\infty \rho_p(r)4\pi r^2dr\,. \tag{11}$$

The integral:

$$\int_0^\infty \rho_p(r)r^2dr = m_2 \tag{12}$$

is the second order moment of the probability density function. Thus finally one has:

$$A_{tot} = 4\pi R^3 m_2/m_3\,, \tag{13}$$

and, under the assumption $A_{tot} >> A_0$, the fragmentation energy E_{frag} reads as:

$$E_{\text{frag}} = 4\pi K R^3 m_2/m_3\,, \tag{14}$$

where K denotes the surface tension coefficient of water.

As is clear, it is enough to know the second and third order moments of the corresponding probability density function and not the density function itself. Their values may be estimated for a sufficiently numerous sample of droplets, provided a method of determining their radii is available. In such a case, after determining radii r_n of N droplets, one would have:

$$m_2 \approx \frac{1}{N}\sum_{n=1}^{N} r_n^{\,2}, \text{ and } m_3 \approx \frac{1}{N}\sum_{n=1}^{N} r_n^{\,3}. \tag{15}$$

This is a fortunate circumstance, since from this point of view the reconstruction of the actual distribution is of secondary importance, and determining ρ from first principles is rather not a simple task.

Measuring the radii of a decent sample of droplets, however, is no trivial task since the droplets are literally volatile objects, short living due to both evaporation and/or merging. As such, one has to estimate the radii indirectly, by determining some variables whose values depend on them or to collect droplets in a way that would allow to determine their radii almost instantaneously. Below we will describe two methods based on the first of the mentioned philosophies and one based on the second one.

3. Determination of the droplets' radii

Determination of radii of droplets can be achieved in several ways. Some limiting estimates can be obtained from measurement of velocity of their uniform fall in the static air. The method is simple enough to use it directly in the field tests. On the other hand, however, in this way one can determine only the lower limit of the radius.

The method that, under some assumptions, can be used for determination of the radii distribution is based on the Fraunhofer diffraction of light on water droplets. We sketch the fundamentals of the method. Although in principle it is quite accurate it can hardly be used in field tests of this type. Therefore it is used rather for calibration of the measuring apparatus that is based on "catching" droplets on a glass plate covered with soot. Although this method does not allow to measure directly the radius of a spherical droplet due to it deformation upon adhering to the plate, the directly measured diameters of adhering droplets can be scaled down thanks to calibration, to give a relatively accurate estimate of the radius of a spherical droplet. On the other hand the apparatus is robust enough to be used in close vicinity of the explosion axis, and therefore applicable in field conditions.

3.1. The fall-velocity method

The method is based on the assumption that due to the microscopic sizes the droplets fall under the influence of only the gravitation force and the Stokes viscosity generated friction. In static air both forces act along the vertical axis and have opposite senses. The velocity of a droplet almost instantaneously achieves the value at which both forces cancel. The condition for the equality of the gravity force P and the Stokes friction R is given by the formula:

$$R = P. \tag{16}$$

The forces are given by the formulae [9]:

$$P = \rho g V \tag{17}$$

and

$$R = 6\pi\, r \eta\, v, \tag{18}$$

where V is the droplet's volume, r – its radius, v – its fall-velocity, ρ – water density, η – dynamical viscosity coefficient of air and g – gravitational acceleration. From Eq. (16) one can obtain the following formula for the droplet's radius with respect to the equilibrium fall velocity v and universal parameters ρ, η and g:

$$r = \sqrt{\frac{9\eta v}{2\rho g}}\,. \tag{19}$$

As such, knowing the fall velocity in principle one can immediately compute the droplet's radius. It is not possible, however, to determine the velocity of an individual droplet. Practically one can determine the fall-velocity of the upper edge of the cloud. This in turn allows one to estimate the lower limit of the radius of the droplets whose number is statistically important.

We report results of such measurements but they are an exercise rather than the source of comprehensive information about the distribution of radii of the cloud's droplets, since the knowledge of the lower edge of the distribution does not allow to compute its moments. Therefore this method cannot provide data necessary for computing the fraction of energy used for fragmentation.

The fall velocity was estimated using a high-resolution video camera Sony HDR-FX1E (image resolution 1440x1080, registration frequency 25 fps). A sample image of the fully developed cloud is shown in Fig. 1.

Fig. 1. Determination of the upper edge of the water-spray cloud with respect to a fixed reference level. The initial stage of cloud's fall is registered.

It is clearly visible that the upper edge of the cloud is quite fuzzy and, consequently, the determination of either its vertical coordinate or the fall velocity cannot be too accurate.

3.2. Method of measuring adhering droplets

In this subsection we describe the methodology of measuring radii of droplets that adhere to a glass plate degreased or covered with soot. The trap-box for collecting and measuring droplets will be described further in this subsection and at the beginning we analyze the basic problems connected with measuring sizes of droplets adhering to the plate and rescaling them to get the sizes of the same droplets being of a spherical shape. In Fig. 2 we show a schematic cross-section of a droplet adhering to a hydrophilic surface (degreased glass) and to a hydrophobic surface (*e.g.* glass covered with soot).

The figure shows schematically deformations of droplets upon adhesion. In the case of the hydrophilic surface, when the adhesion coefficient is larger than the cohesion coefficient (Fig. 2a) the adhesion angle is smaller than 90º, the droplet is considerably flattened and the diameter of the adhesion area is the same as the diameter of the droplet itself and larger than the diameter of the droplet in the air. In the case of the hydrophobic surface, when the adhesion coefficient is smaller than the cohesion coefficient (Fig. 2b), the adhesion angle is larger than 90º, the droplet is only slightly deformed and the diameter of the adhesion area is

smaller than the diameter of the droplet in the air, which, in turn, is smaller than the diameter of the adhering droplet.

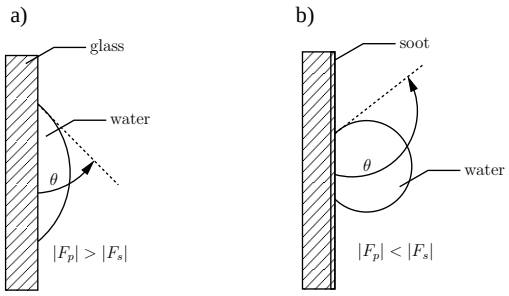

Fig. 2. Variation of the apparent diameter of an adhering droplet measured with a microscope when compared with the diameter in the air: a) degreased glass plate; b) glass plate covered with soot.

The above idealistic considerations do not take into account breaking of the rotational symmetry upon adhesion nor other distortions. This problem will be discussed later. Now we are coming to the description of the droplet trap-box and the methodology of collecting and measuring droplets.

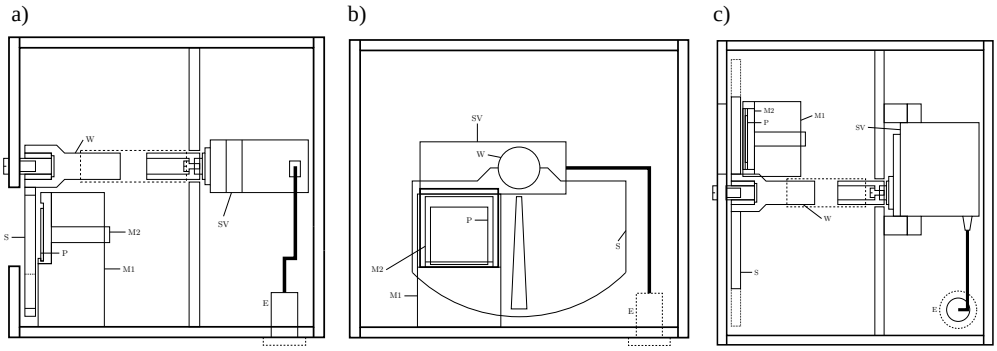

Fig. 3. Droplet-collecting trap-box (P – microscope glass slide – 22 mm by 22 mm by 250 μm), S – shutter, SV – servomechanism, E – electric signal connection , M1 – fixed part of the glass plate fastening element, M2 – its movable part, W – shutter driving shaft connected with the servomechanism): a) side view; b) front view; c) top view.

The triple-view schema of the trap-box is shown in Fig. 3. The trap-box can work in two modes. In the so-called regular mode the shutter S is open for the time t_d starting from the while to after the explosion exposing the whole glass slide P to which droplets adhere.

In the so-called drop-mode the shutter aperture moves across the slide. Its width secures an identical exposition time of 10 ms for all points on the slide. Such a solution makes it possible to collect individual droplets even if their flow is intense. In this mode too the initial moment of the registration can be fixed by the experimenter.

The movable part M2 of the fastening element has hinges allowing one to remove quickly the glass slide from the box and to place it under the microscope. The shorter the time between collecting droplets on the slide and their measurement with a microscope, the smaller the errors following from the change of droplets' size due to evaporation.

The trap-box is used for collecting droplets produced in the act of explosion. Therefore it must be located at a point excluding the danger of damage of the box or its internal parts either by the jet of droplets or by the shock-wave and securing a reasonable (not too large,

since too many droplets collected would merge with each other making diameter measurements impossible) flow of droplets that hit the glass slide as close to the perpendicular as possible.

The above-mentioned objectives can be achieved if the box is mounted on top of an adjustable mast fastened with stays at the height *h* above the ground the same as the water bag is hung and at the distance D from it.

If one is interested in the determination of spatial variation of the radii distribution, the distance D may be varied within the range securing the above mentioned safety measures of the trap-box and measurability of the radii distribution – too small a distance would cause the risk of damage of the box and merging droplets on the glass slide and too large a distance would cause a decrease of the number of registered droplets, making the determination of the radii distribution very difficult due to the paucity of the sample.

3.3. Method of light scattering on water droplets

As was already mentioned, this method is rather difficult for an application in the field. On the other hand, since it is quite accurate, it may be used for determining scaling factors for the measurements performed for the adhering droplets collected in the trap-box. We will give here a concise description of fundamentals of the method.

3.3.1. Fraunhofer diffraction theory

Scattering of light on spherical droplets can be described by the Fraunhofer diffraction theory. A scheme of the diffraction is shown in Fig. 4. One considers laser light shed orthogonally on a screen scattered on a spherical droplet of diameter $d = 2r_0$, whose distance from the screen is L. In such a case circular fringes are observed on the screen.

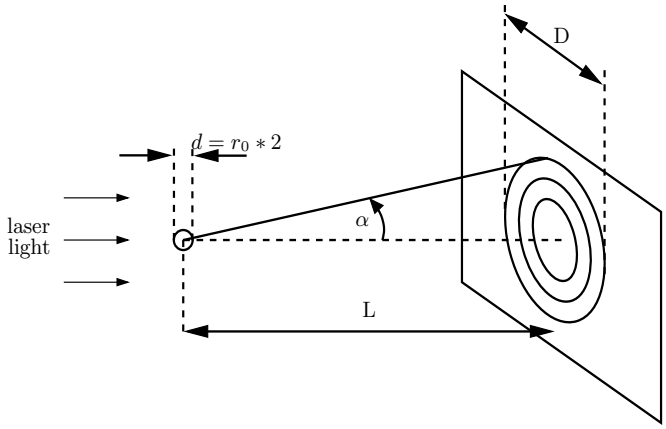

Fig. 4. Schematic view of Fraunhofer diffraction.

The dependence of the intensity *I* of the fringe whose angular distance α from the axis of the incoming beam is given by the formula [10]:

$$I = I_0 \left(\frac{2J_1(kr_0 \sin\alpha)}{kr_0 \sin\alpha} \right)^2 , \tag{20}$$

where J_1 is the first order Bessel function, k is the laser light's wave-number and I_0 is the light-beam's intensity. The angles α for which the dark fringes are observed in the diffraction image are given by the formula:

$$\alpha_k = \frac{p_k \lambda}{\pi d}, \tag{21}$$

where p_k is the k-th zero of the first order Bessel function, λ – denotes the wavelength of the incident light (632.8 nm), and d – the diameter of the aerosol droplet. After inverting the formula with respect to d one has:

$$d = \frac{p_k \lambda \cdot 180}{\pi \alpha_k \cdot \pi}. \tag{22}$$

This is an approximated formula which cannot be improved within the Fraunhofer theory of diffraction assuming a flat disc- scatterer rather than a spherical one.

3.3.2. Mie light scattering theory

A more sophisticated description can be achieved within the theory of light scattering. In the case of uniform spherical scatterers, the Mie theory [11] should be sufficient, although more general theories are also available [12, 13]. In Mie theory, coefficients a_n, b_n, c_n, and d_n describing the amplitudes of the scattered field are obtained from Maxwell equations:

$$a_n = \frac{m^2 j_n(mx)[xj_n(x)]' - j_n(x)[mxj_n(mx)]'}{m^2 j_n(mx)[xh_n^{(1)}(x)]' - h_n^{(1)}(x)[mxj_n(mx)]'}, \tag{23}$$

$$b_n = \frac{j_n(mx)[xj_n(x)]' - j_n(x)[mxj_n(mx)]'}{j_n(mx)[xh_n^{(1)}(x)]' - h_n^{(1)}(x)[mxj_n(mx)]'}, \tag{24}$$

$$c_n = \frac{j_n(x)[xh_n^{(1)}(x)]' - h_n^{(1)}(x)[xj_n(x)]'}{j_n(mx)[xh_n^{(1)}(x)]' - h_n^{(1)}(x)[mxj_n(mx)]'}, \tag{25}$$

$$d_n = \frac{mj_n(x)[xh_n^{(1)}(x)]' - mh_n^{(1)}(x)[xj_n(x)]'}{m^2 j_n(mx)[xh_n^{(1)}(x)]' - h_n^{(1)}(x)[mxj_n(mx)]'}. \tag{26}$$

where m is the refraction coefficient which in the case of water is m = 1.33+0.01i, $x = kr_0$ is the size parameter, r_0 is the droplet's radius, $k = 2\pi/\lambda$ is the incident light wave-number, and λ – its wavelength. Functions $j_n(z)$ and $h_n^{(1)}(z) = J_n(z) + iy_n(z)$ are n-th order spherical Bessel functions. The apostrophes in equations (23–26) denote differentiation:

$$[zj_n(z)]' = zj_{n-1}(z) - nj_n(z); \qquad [zh_n^{(1)}(z)]' = zh_{n-1}^{(1)}(z) - nh_n^{(1)}(z). \tag{27}$$

The relation between Bessel functions and spherical Bessel functions is described by the formulae:

$$j_n(z) = \sqrt{\frac{\pi}{2z}} J_{n+0.5}(z), \tag{28}$$

$$y_n(z) = \sqrt{\frac{\pi}{2z}} Y_{n+0.5}(z), \tag{29}$$

where J_m i Y_m are first- and second-order Bessel functions.

The intensity of the forward-scattered light is given by:

$$Q_{sca} = \frac{2}{x^2} \sum_{n=1}^{\infty} (2n+1)(|a_n|^2 + |b_n|^2). \tag{30}$$

Scattering of the light-beam has axial symmetry. Therefore, the intensity of the scattered light can be represented with a function of the scattering angle only. Results of computations of this function for scattering of laser light of the wavelength 632.8 nm on water-sprays consisting of droplets with radii r_0 =1 μm and 10 μm for the whole range of 0° < α < 180° are shown in Fig. 5. In Fig. 5a plots of intensities of the light scattered on 1μm droplets for depolarized light and two perpendicular polarizations of the incident beam are shown.

Fig. 5b shows analogous plots in the case of scattering on a water-spray consisting of 10 μm droplets. Higher resolution plots for 0° < α < 10° (forward-scattering) and for 170° < α < 180° (back-scattering) in the case of the same spray are shown in Fig. 6a and Fig. 6b, respectively.

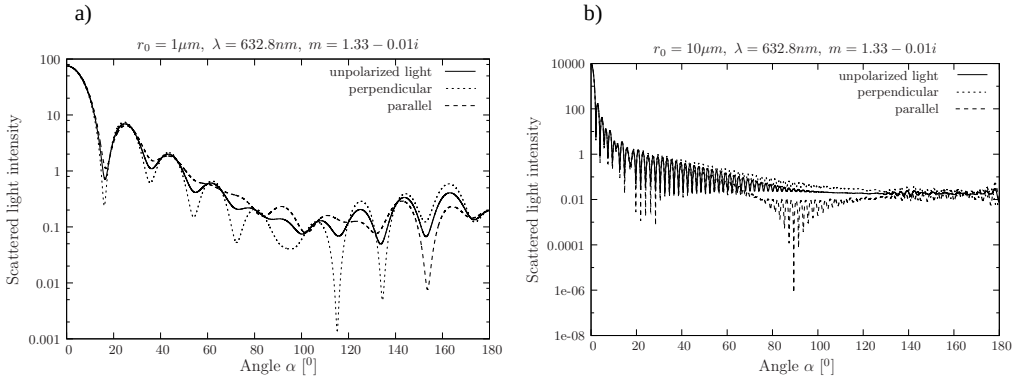

Fig. 5. Plot of the scattered light intensity for: a) 1 μm; b) 10 μm droplets.

As is clearly visible, the intensity of the forward-scattered light is from two to four orders of magnitude larger than the intensity of the back-scattered light irrespective of light's polarization. This implies that measurements should be performed for forward-scattered light. It is also clear that in the case of forward-scattered light its polarization plays a marginal role and, consequently, one can measure the intensity of depolarized light. Since the intensity of the scattered light decreases with square of the distance, one should place detectors close to the sample spray.

Taking the dependence of intensity of the scattered light on the scattering angle one can simulate scattering images for various droplets' radii. Results of such simulation based on Mie theory for the scattering of monochromatic light on water spray are shown in Fig. 7.

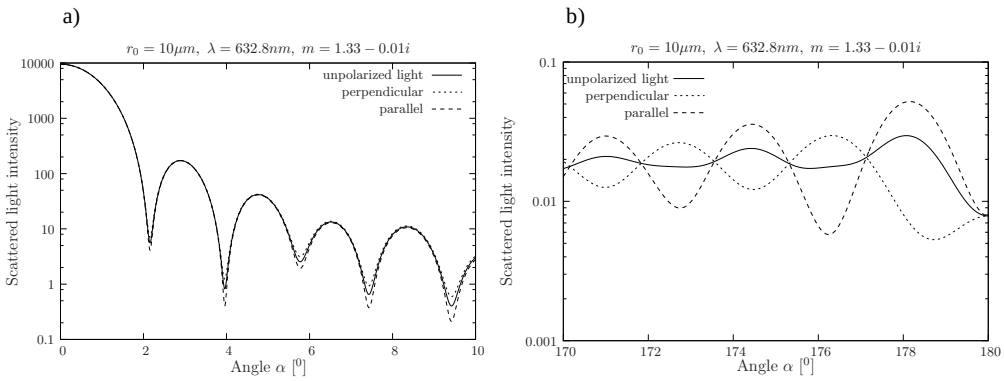

Fig. 6. Plot of: a) the forward-scattered; b) the back-scattered light intensity for 10 μm droplets.

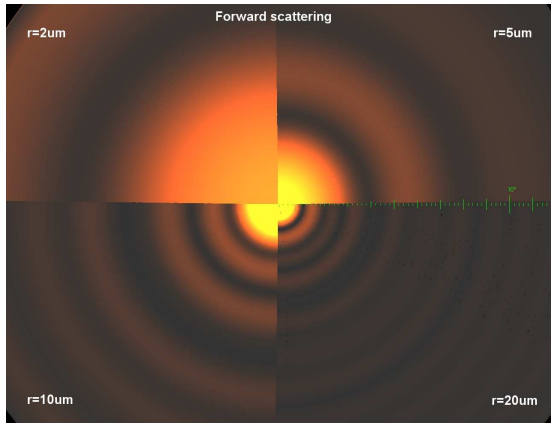

Fig. 7. Simulation of the forward-scattering image for the beam of light with λ = (632 ± 1) nm and sprays consisting of spherical droplets of various radii.

3.4. Recalculating results obtained from microscopic measurements

Purely theoretical recalculation of the trapped droplets' diameters measured with a microscope to obtain corresponding diameters of the same droplets in the air is a task of high complexity. Therefore a less ambitious but sufficiently efficient way was chosen. By comparison of diameters determined from light scattering with those measured by microscope for the same set of droplets produced in laboratory, the scaling coefficient was determined, allowing one to scale the results of the latter type of measurements for the droplets collected in field experiments, where the light scattering methods are not applicable.

Such an approach allows one to combine a field-applicable method giving distorted results with higher accuracy of a method applicable only in a laboratory.

4. Experimental results

In this section results of experiments based on the methods described in Section 3 are presented. We report results obtained in experiments of all three types.

4.1. Measuring droplets using the fall-velocity method

Measurements of the fall-velocity are based on registering the upper edge of a selected part of the spray cloud with a video-camera and processing data from subsequent frames. Typical plots for a dozen of series of such measurements versus time interval (computed from the number of the frame) is shown in Fig. 8a. As is clearly visible, the general shape of the plot of data series is the same for all particular cases. The plots have the same shape: in the initial stage of the spray cloud expansion the height of its upper edge above the ground increases and later begins to decrease. After several seconds the velocity of this decrease stabilizes and the plot is close to a straight line.

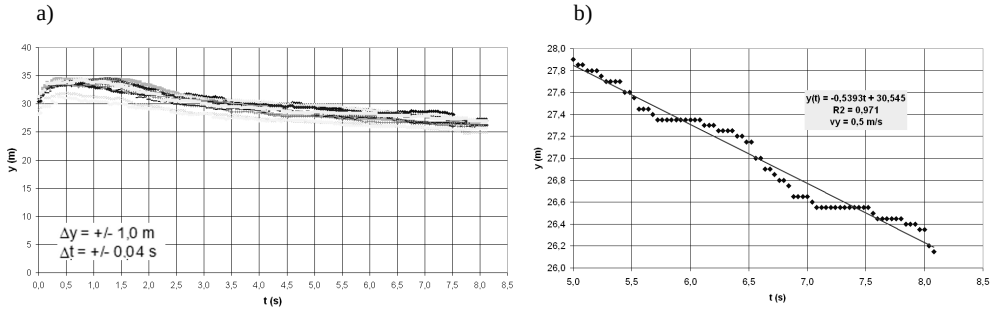

Fig. 8. a) Series of data for the height of the upper edge of 11 selected parts of a water-spray cloud obtained in a test with a water-bag containing 1500 dm^3 of water and scattered with a charge of Emulinit producing an explosion energy of 10.8 MJ. b) A series of values of the height of the upper edge of the spray cloud versus time obtained in a test with a water-bag of 1500 dm^3 of water and a charge of Emulinit producing an explosion energy of 10.8 MJ, shown together with the plot of the linear regression computed with the least squares method. The absolute value of the slope coefficient gives an estimate of the fall velocity, which in this case is about 0.5 m/s.

As experience gained during a series of tests shows, for times exceeding about 5 s after the explosion the fall of the upper edge of the cloud is uniform. Therefore, in all cases the uniform fall-velocity is determined for the time interval from 5 to 8 s after the explosion, since later the cloud becomes too thin to measure the height of its upper edge.

The uniform fall-velocity is obtained as the absolute value of the slope coefficient of the linear regression fitted to the experimental points in the aforementioned time interval using the least squares method. An exemplary plot showing both the experimental points and the computed linear regression is shown in Fig. 8b. Taking into account all experiments, an average diameter of droplets of (140 +/–25) µm diameter has been obtained. This is an estimate for a small fraction of the water-spray. In a way one can say that the method based on measuring the fall velocity allows to detect droplets with diameters of (140 +/–25) µm. The optical method to be discussed in the subsequent Section allows to determine diameters of droplets belonging in general to another fraction. Consequently, a direct comparison of results obtained with both methods would not necessarily be reasonable.

4.2. Measuring trapped droplets using a microscope

This subsection is devoted to measuring with a microscope the diameters of droplets adhering to the glass slide of the trap-box. Two series of tests have been performed: one for degreased slides and another for slides covered with soot.

4.2.1. Preliminary tests

Practical implementation of the program of the experiment is not simple. Therefore the first series of experiments served mainly as the debugger of the program from "good" ideas that turned out to be absolutely impractical due to difficulties not foreseen ahead of time.

Testing various positions and orientations of the trap-box with respect to the axis of explosion allowed to choose efficient configurations. Comparison of tests with droplets collected on the degreased and soot-covered slides had shown that the earlier were of little use due to rapid evaporation of droplets. It was also checked that cooling down the slide to -3 °C was not a remedy since it caused an even larger problem due to the appearance of a mass of artifact condensation droplets.

Only after collecting sufficient experience the second series of tests with the soot-covered slides had been carried on. In this series the collected droplets evaporated as quickly as before but their traces on the soot, corresponding to the adhesion area, could be measured even quite long after the disappearance of the droplets themselves. The soot proved a good medium for "eternizing" droplets' traces, and, consequently, the difficulties following from the fast evaporation of droplets have been removed. As was discussed in Section 3, the diameter of a trace left by the droplet is not identical with that of the droplet itself. However, the scaling factor for determining the diameter of a droplet from the diameter of its trace on the soot has been obtained from parallel measurements in the laboratory of the diameters of traces left by droplets on the soot using a microscope and measurements of diameters of the droplets themselves using the optical methods described in Section 3.

4.2.2. Droplets on soot-covered slides

In this series of tests the water-bag was lowered to 1.7 m. This allowed to place the trap-box in a position allowing almost immediate removal of the glass slide and simultaneously being optimal from the point of view of the flow of droplets. Such a lowering was made possible thanks to hanging the bag from a solid steel frame instead of using a mobile crane. The bags were filled with 1200 dm^3 of water and "stuffed" with an explosive charge weighing 4.5 kg.

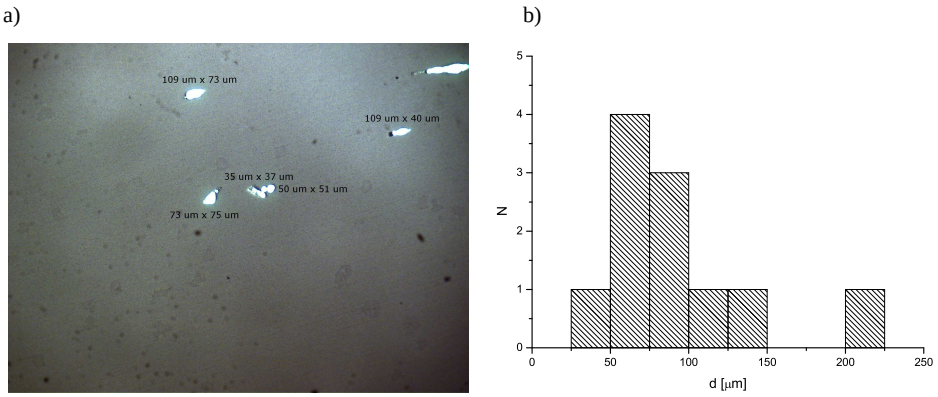

Fig. 9. a) Exemplary image registered for a test with shutter time delay t_o = 100 ms in aperture mode. The water capsule hung 1.7 m above the ground and the trap-box placed at the same height of 8m from the explosion axis. b) The histogram of droplets' diameters for the set of droplets.

The glass slide was covered with a layer of soot by exposing it to the flame of a paraffin candle. As preliminary tests have shown, the thicker the soot layer (the longer exposition to the flame), the smaller the traces left by droplets. Therefore, for the later tests a set of slides with an identical soot layer has been prepared.

It turned out that the shutter opening time 1 s in the regular mode was too long and the slide was covered uniformly with water. Therefore, the drop-mode was used in further tests. Under such conditions, more than a dozen of well separated droplets were registered An image of the registered droplets is shown in Fig. 9a. Again, the number of droplets is large enough to construct a histogram show in Fig. 9b.

In the next test the shutter was opened for 0.3 s working in the regular mode. It allowed to obtain an image of separate traces left by the registered droplets, shown in Fig. 10a.

The large central disc in the center of Fig. 10a is not caused by inhomogeneity of soot layer but follows from inhomogeneous illumination of the slide by the microscope lamp. The histogram corresponding to the droplets shown in Fig. 10a is presented in Fig. 10b.

Another test was performed for the determination of the distribution of droplets' diameters 8 m from the explosion axis in the time interval from 250 to 550 ms after the explosion, which corresponds to a delay time of the shutter of t_o = 250 ms and an opening time of t_d = 300 ms. The resulting histogram is shown in Fig. 11.

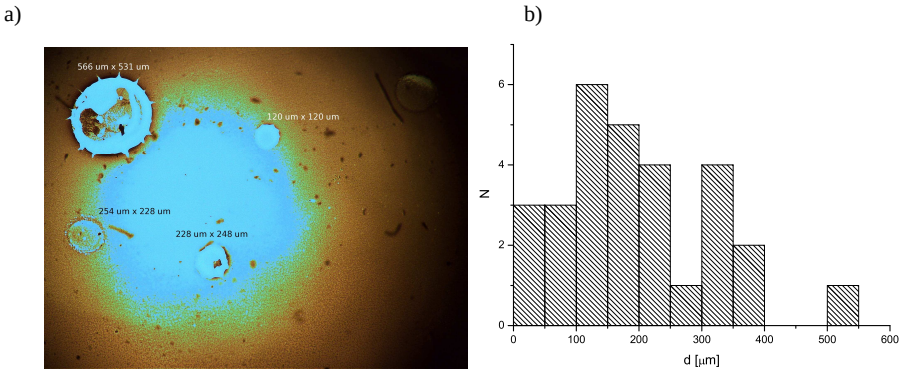

Fig. 10. a) Exemplary image registered for a test with shutter time delay t_o = 50 ms and opening time t_d = 300 ms in the regular mode. The water capsule was hung 1.7 m above the ground and the trap-box was placed at the same height, 8 m from the explosion axis. b) The histogram of droplets' diameters for the set of droplets.

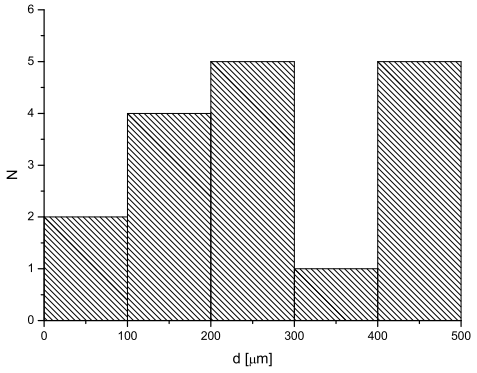

Fig. 11. The histogram of droplets' diameters for the set of droplets registered for a test with shutter time delay t_o = 250 ms and opening time t_d = 300 ms in the regular mode. The water capsule was hung 1.7 m above the ground and the trap-box was placed at the same height 8 m from the explosion axis.

Comparison of histograms from Fig. 10b and Fig. 11 shows that the flow of aerosol in the time interval 50 ms < t < 350 ms is about twice larger than in the time interval 250 ms < t < 550 ms. It is also clear that the droplets reaching the trap-box in the earlier interval are smaller.

The next test was performed for the time interval 150 ms < t < 450 ms, the explosive charge enlarged to 5.5. kg and the trap-box placed 9 m from the explosion axis. The height above the ground of both the water-bag and the trap-box was equal to 1.7 m as in the previous tests. The image of the registered droplets is shown in Fig. 12a and the corresponding histogram of the diameter is given in Fig. 12b.

It is clear that the increase of the explosive charge resulted in a larger number of smaller droplets. This is in accordance with the expectation that larger explosion energy results in more efficient pulverization. After increasing the registration time in a subsequent test by 100 ms, the slide was almost completely covered with water like in the first test with t_d = 1s. One can conclude on this ground that the 9 m from the explosion axis the aerosol flow generated by 5.5 kg explosive charge is the largest in the interval 450 to 550 ms after the explosion.

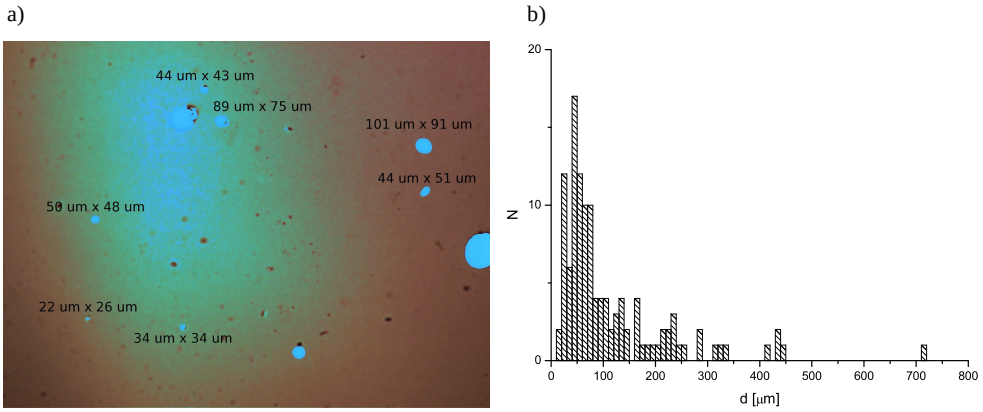

Fig. 12. a) Exemplary image registered for a test with shutter time delay t_o = 150 ms and opening time t_d = 300 ms in the regular mode. The water capsule was hung 1.7 m above the ground and the trap-box was placed at the same height, 9 m from the explosion axis and the explosive charge enlarged to 5.5 kg. b) The histogram of droplets' diameters for the set of droplets

4.2.3. Corrections for non-circularity of trapped droplets

Part of the droplets enters the trap-box with non-zero component of velocity tangent to the glass slide. As a result the shapes of the adhering droplets are rather elliptic than circular.

In such a case the diameter of the virtual circular trace d was obtained from the lengths of the main semi-axes a and b of the ellipse as the geometric average:

$$d = 2\sqrt{ab}\,. \tag{31}$$

Only after this recalculation the correction for recalculating the trace diameter on the glass-slide was used for determining the diameter (or radius) of the same droplet in the air.

4.3. Measuring the diameters of aerosol droplets using forward-scattered light

Determining the radii (diameters) of aerosol droplets using a glass slide and microscope requires support with a calibration procedure due to unknown adhesion angles of droplets to the slide. To work-out correcting procedures, the diameters of droplets in the air have been

measured using forward-scattered laser light and compared with the diameters of identically produced droplets adhering to the glass slide.

A schematic view of the experiment with light scattering is shown in Fig. 13. Droplets produced by an atomizer have been illuminated with a light-beam emitted by the 15 mW He-Ne laser, and expanded 20 times transversally by the expander to cross a sufficiently large part of the spray. Monochromatic light was used for the sake of simplicity of interpretation of the results.

The screen made of a sheet of paper was placed about 1 m from the stream of aerosol. The extended light-beam was focused on the screen which was perforated at the focal point to quench the principal beam that was dissipated inside the cavity constructed behind the screen.

The diffraction image was photographed with a Nikon Body 3D camera at an inclination angle 30° with respect to the beam's axis from a distance of 30 cm from the screen. Due to dynamic evolution of the image the pictures have been taken in the multi-shot mode. The distances were chosen to optimize the quality of the pictures.

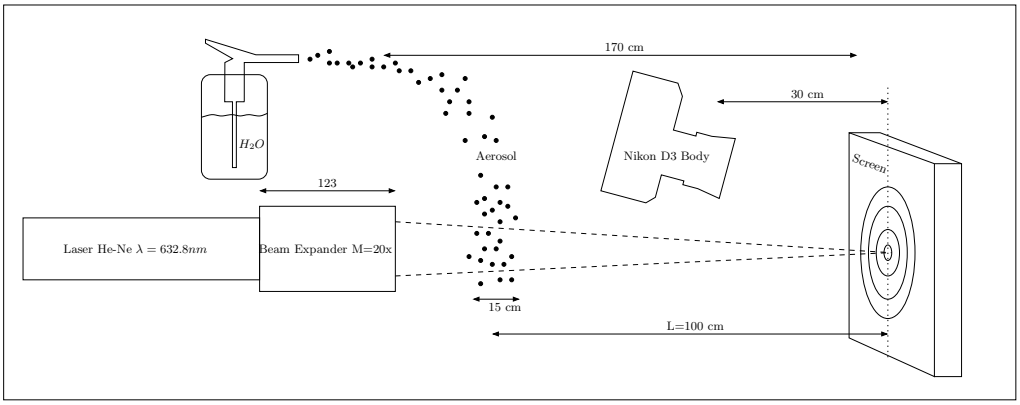

Fig. 13. A scheme of the diffraction experiment.

4.3.1. Sample images of the scattered light

In Fig. 14 an image of forward scattered light taken by a camera in a dark room is shown.

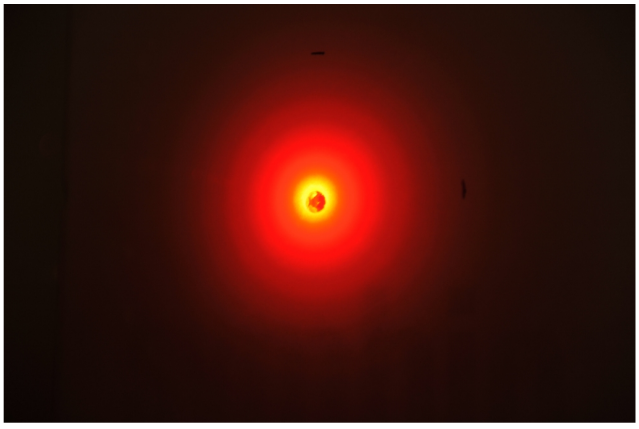

Fig. 14. An image with quenched principal beam.

The large intensity of the principal beam resulted in saturation of the CMOS matrix and, consequently, in lowering general sensitivity and poor visibility of interference fringes.

Therefore, the principal beam has been quenched, which allowed to take the picture with higher sensitivity, which resulted in better visibility of interference fringes by several orders.

4.3.2. Analysis based on the Fraunhofer diffraction theory

To determine diameters of aerosol droplets d, the radii r_k of subsequent dark fringes have been measured in terms of pixels. After recalculating into standard length units the radii have been transformed into the corresponding diffraction angles α_k. For each of the angles the estimate of d was computed. The average of the estimates was taken as the estimate of the "standardized" droplet diameter.

Table 1. Analysis of fringes from a particular picture. Recalculation was done on the equivalence of 1579 pixels and 110 mm, which gives the coefficient 0.069664 mm/pixel.

Min no k	Root	r_k [pxl]	r_k [mm]	α_k [°]	d [μm]
1	3.8317	226	15.74	0.90	49.01
2	7.01558	335	23.34	1.34	60.55
3	10.17346	462	32.18	1.84	63.68
4	13.32369	548	38.18	2.19	70.32
5	16.47063				

The analysis gives the average value of d = 64 μm.

4.3.3. Analysis based on the Mie light scattering theory

The Mie light scattering theory described in subsection 3.5.2 fits better the obtained image. To determine diameters of droplets one has to solve the Mie inverse problem. To achieve this objective one has to determine from the photograph the dependence of the light intensity I on the scattering angle α. In the next stage one has to fit to this numerically defined function a function similar to that from Fig. 6a.

Since the pictures had been taken at the angle 30° from the normal to the screen, the circular fringes were deformed into elliptic ones. Therefore applying a transformation compensating this deformation was necessary. The transformation is relatively simple since it consist in extension of the short axes of the elliptic fringes to make them identical with the corresponding long axes. The result of such transformation is shown in Fig. 15.

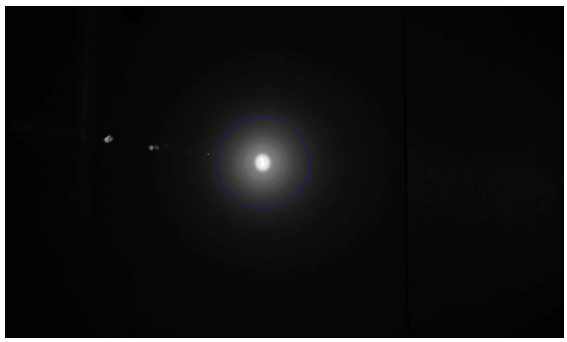

Fig. 15. The corrected picture with deformation removed.

The next stage of the procedure consists in determining the position of the center of the circular interference fringes and verifying its accuracy by placing circles with centers in that point. plotting the light intensity as a function of the distance from the center in terms of pixels. The next step consists in precise determination of the center of the interference fringes. The result is verified.

The dependence of the light intensity on the distance from the center of fringes is shown in Fig. 16a. Maxima and minima are barely visible and it is not possible to fit the Mie curve to such a plot. Variability of intensity of the scattered light is much better visible in the plot of the derivative of the light intensity with respect to the radial distance. This is shown in Fig. 16b.

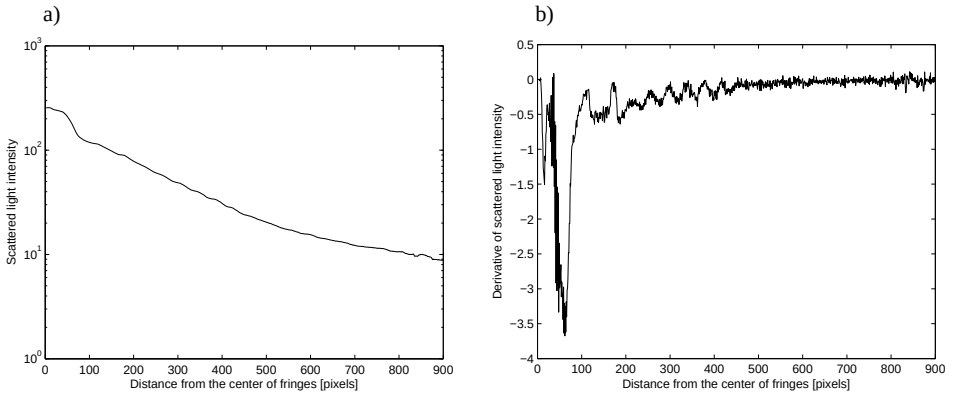

Fig. 16. a) Scattered light intensity and b) derivative of the scattered light intensity as a function of the radial distance from the center of fringes.

4.4. Correction of diameter distributions determined from microscopic measurements

To determine coefficients allowing to scale the results of direct measurements of droplet diameters with the microscopic method, results of estimates of diameters from the light scattering method have been compared with the results of microscopic measurements of diameters for the same set of droplets. This sort of comparison has been performed both for droplets collected on a degreased glass sidle and a glass slide covered with sooth.

For the etalon sample the forward-scattering method has given diameters 64 μm ± 10 μm. For the degreased slide the corresponding values are 400 μm ± 115 μm (Fig. 17(a)). The scaling factor in this case was estimated for s_{1a} = 6.25. For the sooth-covered glass slide the values of diameters were 165 μm ± 41 μm (Fig. 17(b)), and the corresponding scaling factor was estimated as s_{2a} = 2.58.

After multiplying the microscopically measured diameters by the scaling factors s_{1a} and $s_{2a,}$ respectively, new histograms were constructed (Fig. 18) and Gaussian curves are fitted. As is clear, the fitting is definitely not satisfactory and other model distributions must be used.

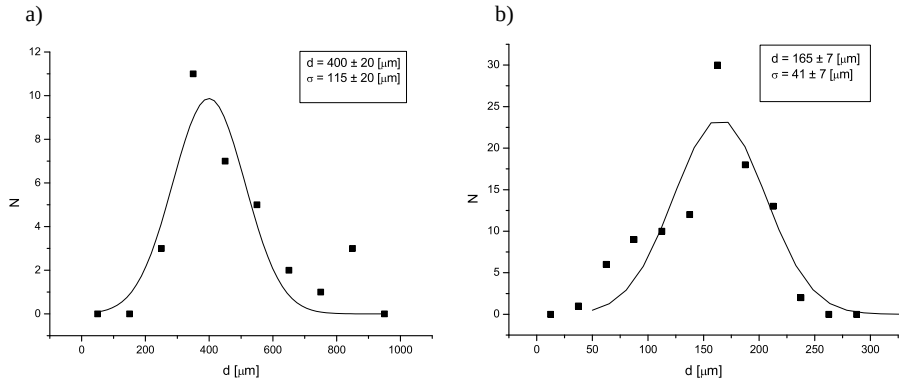

Fig. 17. Histogram of water droplets' diameters: a) registered on a degreased glass sidle; b) registered on a glass slide covered with sooth.

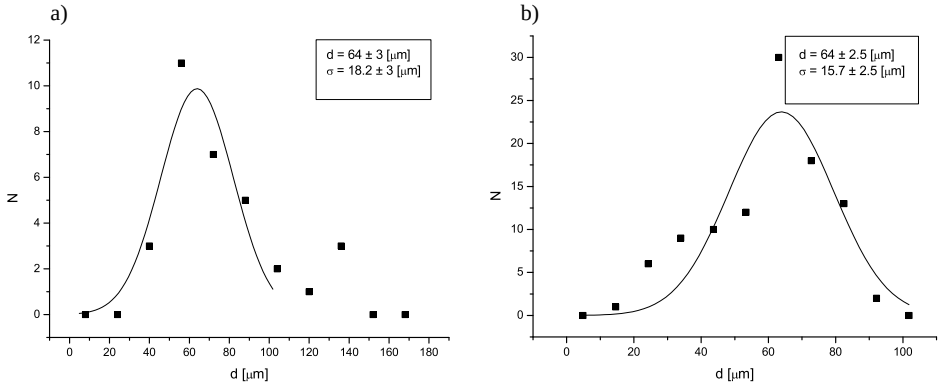

Fig. 18. Rescaled histograms for experiments shown in Fig. 17.

5. Distribution of the droplets' radii

Experimental data are used for determining values of parameters of the model distribution of radii of the form:

$$n(r) = N_0 r^{\mu} \exp\left(-\frac{\mu}{a_0} r\right), \tag{32}$$

where r denotes the droplet's radius, N_0 is a normalization factor and μ, a_0 are parameters of the distribution. The normalization factor is of the form:

$$N_0 = \left[\left(\frac{a_0}{\mu}\right)^{\mu+1} \Gamma(\mu+1)\right]^{-1}. \tag{33}$$

The expectation value of r for this distribution is given by:

$$\langle r \rangle = \left(\frac{a_0}{\mu}\right)(\mu+1), \tag{34}$$

and its standard deviation is:

$$\sigma = \left(\frac{a_0}{\mu}\right)\sqrt{\mu+1}\,. \tag{35}$$

Parameters had been determined for a number of experimental data.

Table 2. Parameters of the model radii distributions (32) for five various experiments.

Water volume V [m^3]	Explosion energy E_{ex} [MJ]	E_{ex}/V. [MJ/ m^3]	a_0	μ	N_0	<r> [μm]	σ [μm]	Corr.
0.6	4.4	7.3	17.9	1.0	0.8	35.5	25.1	0.616
0.6	7.3	12.2	5.7	2.8	8.8	7.7	3.9	0.990
1.2	10.8	9.0	23.5	2.0	1.6	35.6	20.7	0.993
1.2	13.1	10.9	8.1	2.0	14.0	12.2	7.0	0.997
1.2	16.6	14,8	5.2	2.0	8.0	9.1	5.2	0.998

6. Determination of pulverization energy from the droplet radii distribution

Even having relatively few radii of droplets one can estimate the m_2 and m_3 moments with reasonable accuracy and, consequently, determine the energy used for fragmentation of water, using Eq. (14). Such estimates for a number of experiments are shown in Table 3.

Table 3. Pulverization energy.

V [m^3]	E_{expl} [MJ]	E_{expl}/V [MJ/ m^3]	E_{frag} [kJ]	E_{frag}/E_{expl} [%]
0.6	4.4	7.3	2.8	0.064
0.6	7.3	12.2	11.2	0.153
0.6	7.3	12.2	2.0	0.027
0.6	7.3	12.2	18.6	0.255
1.2	10.8	9.0	3.6	0.033
1.2	10.8	9.0	3.0	0.028
1.2	13.1	10.9	7.5	0.057
1.2	13.1	10.9	8.3	0.063
1.2	16.6	13.8	36.7	0.221
1.2	16.6	13.8	13.2	0.080
1.2	16.6	13.8	19.0	0.114

As is clear, this energy is not particularly impressive and varies around 0.1% of the total explosion energy. On the one hand it is not too surprising since water is not a highly cohesive medium. On the other hand, even an essential increase of this energy would not affect the amount of energy used for acceleration.

7. Conclusions

As was demonstrated, measuring the distribution of droplets' radii is not a trivial task due to evaporation and deformation of droplets by adhesion forces. Therefore the obtained results should be treated as rather rough estimates that can vary within an order of magnitude. It is not clear yet how much of this variability should be ascribed to the actual variability of the fraction of energy dissipated into the pulverization channel and how much to errors in the estimates connected with, say, under-representation of smallest droplets, with inaccuracies of the rescaling procedure *etc*.

Nevertheless the estimates show that the energy fraction dissipated into the fragmentation channel is much smaller than the fractions dissipated into the two remaining channels. This, in

turn, means that relatively large increase of fragmentation energy and pulverization of water into essentially smaller droplets should not influence the explosive acceleration of water. The only problem that has to be solved would be finding a mechanism that would allow one to pump more energy into the fragmentation channel.

Acknowledgments

The paper is partially supported by the Grant of Polish Ministry of Science and Higher Education 8003/R/T00/2007/03.

References

[1] Z. Liu, A. K. Kim, D. Carpenter: "Extinguishment of large cooking oil pool fires by the use of water mist systems". *Combustion Institute/Canada Section Spring Technical Meeting*, May 9–12, 2004, pp. 1–6.

[2] D. Dierdorf, J. Hawk*:* "Blast Initiated Deluge System. An Ultra-High-Speed Fire Suppression System Air Force". *Research Laboratory Preprint:* AFRL-ML-TY-TP-2006-4511, 2006.

[3] G. Śmigielski, D. Lewandowski, R.S. Dygdała, K. Stefański, W. Urbaniak: "Water capsule flight – a theoretical analysis, experimental setup and experimental verification". *Metrol. Meas. Syst*., vol. XVI, no. 2, 2009, pp. 313–322.

[4] W. Teie: *Firefighter's handbook of wildland firefighting*. Dear Valley Press Recue CA, 1994.

[5] E. Kuhrt, J. Knollenberg, V. Martens: "An automatic early warning system for forest fires". *Annals of Burns and Fire Disasters*, no. 14, 2001, pp. 151.

[6] K. Stefański, D. Lewandowski, R. Dygdała, G. Śmigielski, M. Kaczorowski, M. Ingwer-Żabowska: "Explosive formation and spreading of water-spray cloud – theoretical models and experiments". *International Conference on Metrology of Environmental, Food and Nutritional Measurements 2nd IMEKO TC19 Conference on Environment Measurement*, Budapeszt, 2008.

[7] G. Śmigielski, R. Dygdała, K. Stefański, D. Lewandowski, W. Urbaniak: "Measuring Shock-Wave Parameters During Explosive Water-Spray Production". *Proceedings of the Conference Metrology in Production Engineering*, Poznań, 2009.

[8] S.V. Stebnovskii: "Pulsed Dispersion as the Critical Regime of Destruction of a Liquid Volume". *Combustion, Explosion, and Shock Waves*, vol. 44, no. 2, 2008, pp. 228–238.

[9] K. Sierański, K. Jegierski, B. Kołodka: *Physics Formulae and Laws with Expalanations.* Oficyna wydawnicza SCRIPTA Wrocław, 2005. (in Polish)

[10] F. Jenkins, H. White: *Fundamentals of optics.* 4th edition, MCGraw-Hill INC, 1976.

[11] G. Mie: *Annalen der Physik*, no. 25, 1908, pp. 377–445.

[12] M. Born, E. Wolf: *Principles of optics*. Pergamon Press Oxford, 1970.

[13] C.F. Bohren, D.R. Huffman: *Absorption and scattering of light by small particles*. Wiley, 1998.